

**Coating Particles with Alumina Nanolayers
Utilizing Atomic Layer Deposition
in a Fluidized Bed Reactor**

by

JEFFREY R. WANK

B.A. University of Colorado, 1998

A thesis submitted to the
Faculty of the Graduate School of the
University of Colorado in partial fulfillment
Of the requirements for the degree of
Doctor of Philosophy
Department of Chemical Engineering

2003

UMI Number: 3087592

PREVIEW

UMI[®]

UMI Microform 3087592


Copyright 2003 by ProQuest Information and Learning Company.
All rights reserved. This microform edition is protected against
unauthorized copying under Title 17, United States Code.

ProQuest Information and Learning Company
300 North Zeeb Road
P.O. Box 1346
Ann Arbor, MI 48106-1346

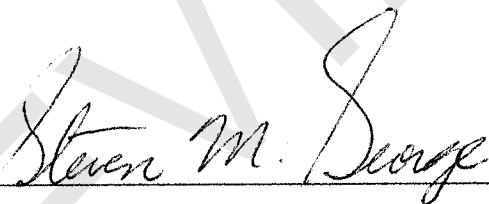
This thesis entitled:
Coating Particles with Alumina Nanolayers Utilizing Atomic Layer Deposition in a
Fluidized Bed Reactor

Written by Jeffrey R. Wank

Has been approved for the Department of Chemical Engineering:



Alan W. Weimer



Steven M. George

Date: April 17, 2003

The final copy of this thesis has been examined by the signatories, and we find that
both the content and the form meet acceptable presentation standards of scholarly
work in the above mentioned discipline.

Abstract

Wank, Jeffrey R. (Ph.D., Chemical Engineering)

Coating Particles with Alumina Nanolayers Utilizing Atomic Layer Deposition in a Fluidized Bed Reactor

Dissertation directed by Alan W. Weimer

There is a current need to provide simple methods to place conformal, pinhole-free, nanoscale-thickness films on fine particles. Such processing can be done using atomic layer deposition (ALD) in a fluidized bed reactor, as will be shown in this thesis. This work is the first application of ALD to coat bulk quantities of fine powders. A fundamental understanding of the fluidization of fine cohesive particles at reduced pressure along with the ALD processing of these particles is the major focus of this thesis. The applications for such nanocoated particles are broad and can be found in many different areas of materials science including microelectronics, defense, biomedical, consumer products, advanced materials, and others.

The minimum fluidization velocity (u_{mf}) of fine cohesive particles at reduced pressure can be calculated using a balance of forces method. Two additional forces are added to a general force balance on a particle with an upward gas flow under vacuum conditions. The final equation is a quadratic in u_{mf} , and can be used to accurately describe u_{mf} for a variety of particle sizes, shapes, and densities. Additionally, as fine particles are coated with an alumina film, the cohesive forces between the particles will change. For the particles of interest in this thesis, the change in the cohesive force is small.

Experiments for alumina deposition on $1.5 \cdot 10^{-4}$ m (150 μ m) diameter nickel particles, several different sized boron nitride (BN) particles (from $5 \cdot 10^{-6}$ to $1.5 \cdot 10^{-4}$ m (5 to 150 μ m) average diameter), and fine ($\sim 5 \cdot 10^{-6}$ m (5 μ m)) iron particles were conducted using trimethylaluminum (TMA) and water as dosing reagents at 450 K. Successful deposition of alumina films, with thickness controllable at the angstrom level, was observed based upon TEM imaging, ICP-AES, XPS, particle size distributions, surface area analysis, and WDS imaging. Nickel particles are coated quite easily. For BN platelet particles, a small exposure ($3.25 \cdot 10^2$ Pa·s ($2.5 \cdot 10^6$ L)) of the reagent gases will coat the edge planes only. A larger dose of $1.3 \cdot 10^4$ Pa·s ($1 \cdot 10^8$ L) will coat the entire particle. After 10 ALD cycles, the exposure can be lowered back to $1.3 \cdot 10^2$ Pa·s ($1 \cdot 10^6$ L) as the film is then growing on alumina and not BN. Improved interfacial adhesion between epoxy and the filler material is noted for alumina-coated BN particles. Nanocoated iron particles show improved oxidation resistance relative to uncoated particles, as long as the film is greater than $2.5 \cdot 10^{-9}$ m (25 Å) thick.

Acknowledgements

First I would like to thank my advisors Alan Weimer and Steven George for their wonderful insight and guidance. Without them this thesis certainly would not have been possible.

Second I would also like to thank my sources of funding: Department of Education Graduate Assistance in Areas of National Need (GAANN), NSF Center for Composite Materials, and ALD Nanosolutions, Inc.

I would like to extend special thanks to Fred Luiszer and John Drexler in the Department of Geology's Laboratory for Earth and Geophysical Sciences (LEGS). Fred and John were instrumental in developing methods for analyzing thin films on fine powders. Also, Ron Goldfarb at NIST-Boulder was instrumental in developing an understanding of the iron magnetization properties. Lastly, Ying-Bing Jiang at the University of New Mexico's TEM laboratory provided us with some special insights into the properties of our films.

The Instrument shop personnel including Willy Groethe, Scott Whitehead, Dana Hauschulz, Dennis Burcham, and Dragan Mejic all deserve a hearty thank you. Jim Kastengren in the CIRES shop, as well as the entire Allen Scientific Crew, also deserve big thanks. Busch Semiconductor in Colorado Springs rebuilt all the vacuum pumps, and kept us operating smoothly.

The Weimer and George research groups both deserve a big thank you for the assistance they provided. Specific thanks go to Karen Buechler for work with the TGA, Chris Gump for assistance with the surface area instrument, Luis Hakim for

assistance with the Visisizer, and John Ferguson for generally putting up with me (and helping with all the BN work).

Lastly, none of this would have been even remotely bearable if it were not for my wife Katherine and son David. There is no way that I could have made it through this without them. They are my inspiration.

PREVIEW

List of Tables.....	ix
List of Figures.....	x
Chapter 1. Introduction.....	1
1.1 Fluidized bed reactors.....	1
1.2 Coating Fine Particles By CVD In A Fluidized Bed Reactor.....	4
1.3 Atomic Layer Deposition.....	10
1.4 Thermal Diffusivity of Filler-Epoxy Composites	11
1.5 Protecting the Surface of Fine Metal Particles from Oxidation.....	12
1.6 Transient Voltage Surge Suppression.....	13
1.7 Scope of Thesis.....	14
1.8 References.....	15
Chapter 2. Vibro-Fluidization of Fine Powder at Low Pressure.....	24
2.1 Abstract.....	24
2.2 Introduction.....	25
2.3 Experimental Setup.....	27
2.4 Derivation of Force Balance.....	32
2.5 Sensitivity.....	45
2.6 Discussion.....	45
2.7 Conclusions.....	54
2.8 Acknowledgements.....	54
2.9 Appendix 1- Calculation of Sphericity	54
2.10 Definition of Terms.....	54
2.11 References.....	57
Chapter 3. Nanocoating 150 Micron Nickel Powders.....	61
3.1 Abstract.....	61
3.2 Introduction.....	62
3.3 Experimental.....	63
3.4 Results and Discussion.....	70
3.5 Conclusions.....	76
3.6 Acknowledgements.....	78
3.7 References.....	79
Chapter 4. Nanocoating 10 Micron Boron Nitride Powders.....	82
4.1 Abstract.....	82
4.2 Introduction.....	83
4.3 Experimental.....	87

4.4 Coating Different Sites on BN Platelets.....	97
4.5 Ex-Situ FTIR Spectroscopy.....	105
4.6 Dynamic Aggregation of BN Particles During Fluidization.....	109
4.7 Application of Coated BN as a Filler Material.....	116
4.8 Conclusions.....	121
4.9 Acknowledgements.....	122
4.10 References.....	122
Chapter 5. Nanocoating 5 Micron Iron Powders.....	128
5.1 Abstract.....	128
5.2 Introduction.....	129
5.3 Experimental.....	129
5.4 Coating Iron Particles With Alumina.....	145
5.5 Oxidation Prevention.....	150
5.6 Magnetic Properties of Coated Iron Particles.....	158
5.7 Conclusions.....	158
5.6 Acknowledgement.....	158
5.7 Appendix 1: Calculation of Film Thickness from ICP-AES Data.....	159
5.8 References.....	159
Bibliography	163
Appendix 1. Operating the fluidized bed for atomic layer deposition.....	170
A1.1 Operation.....	170
A1.2 Alternative Operational Methods.....	183
A1.2 Future Recommendations.....	187
Appendix 2. Electrical and Mechanical Systems.....	188
A2.1 Electrical and Computer Wiring/Hardware for Labview.....	188
A2.2 Labview Programs.....	190
A2.3 System Power.....	205
A2.4 System Mechanical Considerations.....	207

List of Tables

3.1	Area of Nickel and Aluminum peaks as determined by XPS. A= area of a specific peak.....	72
4.1	Different powder sizes used in this work. Notes: * HCV BN powder is comprised of submicron crystals that are agglomerated into $7 \cdot 10^{-6}$ - $11 \cdot 10^{-6}$ m (7-11 μm) aggregates; † Thermagon BN is comprised of approximately $5 \cdot 10^{-6}$ - $10 \cdot 10^{-6}$ m (5-10 μm) BN platelets pre-sintered into $150 \cdot 10^{-6}$ m (150 μm) aggregates.....	109
4.2	Thermal conductivity, ICP-AES data, calculated thickness, and peel strength data for $150 \cdot 10^{-6}$ m (150 μm) BN aggregates coated with alumina.....	117
5.1	ICP-AES results as a function of the number of AB cycles performed, with calculated film thicknesses.....	147
A1.1	Pressures against flowrate with main conductance limiter fully open.....	180
A1.2	Pressures versus flowrate with main conductance limiter throttled.....	181

A1.3	Pressures versus flowrate during a dose, dosing conductance limiters fully open, main conductance limiter throttled shut.....	181
-------------	-------------------------------------------------------------------------------------------------------------------------------	-----

List of Figures

1.1	Illustration of particle coating via CVD. As the precursor reagents are fed into the reactor, they react in the gas phase producing small crystallites of the film material. These smaller crystallites may combine before coming into contact with the substrate, or form directly on the substrate. This leads to non-conformal, granular coatings.....	6
1.2	Graphical representation of ALD. The first reactant is admitted into the chamber, transforming the existing first surface functional group into a second functional group. The next reactant is admitted into the chamber, giving back (in the case of film growth) the original surface functionality.....	11
2.1a	Figure 2.1a is a schematic of the experimental apparatus. (1)- mass flow controller. (2)- vacuum pump. (3)- reactor vessel. (4)- powder. (5)- porous glass frit, distributor plate. (6)- vibromotors. (7)- differential pressure detectors.....	28
2.1b	Figure 2.1b shows the mounting apparatus.....	29

2.2a	An image taken with the VisiSizer™ system. The software is calibrated such that only particles appearing very dark (the ones that are in focus) are counted.....	31
2.2b	The next image in sequence; this image was taken approximately 1/30 th of a second after Figure 2.2a.....	31
2.3	Minimum fluidization velocity vs. pressure as calculated from equation 2.23 for PT180, aggregates of $8 \cdot 10^{-5}$ m. Also shown is calculated u_{mf} from[13].....	46
2.4	Aggregate size of PT180 at $4 \cdot 10^3$ Pa (30 Torr) vs. vibration level, $1.3 \cdot 10^{-2}$ m/s N ₂ flowrate, changing frequency between 60 and 20 Hz.....	51
2.5	Bed differential pressure vs. gas velocity, atmospheric pressure, PT180.....	52
2.6	Bed voidage at minimum fluidization vs. vacuum level for PT180 BN powder. The initial bed height was $8 \cdot 10^{-2}$ m. The lines represent the best fit of the data to a logarithmic function.....	53
3.1	A simplified schematic diagram of the ALD-FBR apparatus for coating	

	nickel particles.	64
3.2	Minimum fluidization velocity versus pressure for $150 \cdot 10^{-6}$ m (150 μ m) nickel particles. Solid Diamonds are data points, Open square is the operating point, and the grey curve is calculated using the equations in [20] and [19]......	66
3.3	Image of fluidizing $150 \cdot 10^{-6}$ m (150 μ m) nickel particles. Image taken by using the laser imaging system described in Chapter 2. Particles are freely fluidizing without agglomeration. Some particles in the image appear to be on top of each other, but that is due to their position in 3 dimensional space while the image is two dimensional.....	67
3.4	Dosing scheme for coating $150 \cdot 10^{-6}$ m (150 μ m) nickel particles. Base pressure is around 253 Pa (1.9 Torr) with N ₂ flow.....	69
3.5	TEM images of Al ₂ O ₃ coated Ni particles. The first picture shows 25 AB cycles, yielding $2.3 \cdot 10^{-9}$ m (2.3 nm). The second picture shows 50 AB cycles, yielding $4.0 \cdot 10^{-9}$ m (4.0 nm).....	71
3.6	Graphical representation of ICP-AES calculated thickness versus the number of AB cycles performed. The slope of the line is approximately	

	one, indicating that approximately $1 \cdot 10^{-10}$ m (1 Å) of Al ₂ O ₃ is being deposited per cycle. Error bars were created by taking the high and low values for observed particle diameters (see Figure 3.8).	74
3.7	Figure 3.7a shows the WDS pattern for aluminum. Figure 3.7b is a simple SEM image of the same frame of Nickel particles.....	75
3.8	Figure 3.8. Normalized particle size distributions for $150 \cdot 10^{-6}$ (150 μm) fine nickel particles, uncoated and coated with 100 AB cycles of alumina....	77
4.1	Figure 4.1. Thermal conductivity of composite BN/Alumina as the alumina film thickness increases. Heat transfer shown is through basal plane of BN.....	85
4.2	Schematic for coating BN particles by ALD in a fluidized bed reactor.....	87
4.3	System response to doses of both water and TMA. There is no fluidizing gas flow.....	90
4.4	Minimum fluidization velocity for coated and uncoated particles. After a few monolayers, the alumina is the dominant feature for Van Der Waals forces. However, the differences for the cohesive forces of attraction between coated and uncoated particles is only 8%. The operating point is at 66.7 Pa (0.5 Torr) and $40 \cdot 10^{-2}$ m/s.....	92

4.5	Image of PT180 during fluidization. The bar is 341 μm long. As can clearly be seen, primary particles aggregate during fluidizing conditions.....	95
4.6	Picture of a BN particle, in the form of a flat plate, looking at the side of the plate. All around the edges, hydroxyl species exist that can be used for ALD chemistry. Basal planes initially have only lone pair electrons, requiring a Lewis acid-base pair to begin the reaction.....	97
4.7	PPM aluminum vs. dose time for very short dosing times. This graph displays the uptake of aluminum on the edge planes only as the dosing time increases.....	99
4.8	TEM image of BN particle coated on edge only. No film exists on the entire basal plane, but evidence of a film on the edge can be seen.....	101
4.9	Complete uptake curve for alumina on BN particles. To coat the edges, the exposure required is $1.3 \cdot 10^2 \text{ Pa}\cdot\text{s}$ (10^6 L). Coating the entire particle requires $1.3 \cdot 10^4 \text{ Pa}\cdot\text{s}$ ($1 \cdot 10^8 \text{ L}$).....	102

4.10	Doses during a changing exposure experiment. The first 10 doses of this experiment (the last 3 of the first 10 are shown) are $1.3 \cdot 10^4$ Pa·s (10^8 L); the next 90 doses are $1.3 \cdot 10^2$ Pa·s (10^6 L) (only 2 of these doses are shown).....	104
4.11	Ex-situ FTIR difference spectrum of BN powder after 11 cycles. Peak at approximately 920 cm^{-1} is associated with growth of alumina on BN powder.....	106
4.12	FTIR spectrum of pure BN powder with varying coating thicknesses of alumina. Notice the two large peak areas near 1100-1600 and 800-900 wavenumbers in the 0 cycle spectrum; these two peaks are bulk Boron Nitride features.....	108
4.13	Figure 4.13. Particle size distribution for several coating thicknesses of PT180™. No size distribution shift in the PSD is observed beyond that observed for processing with no coating (200 B cycles), indicating that the particles do not remain bound in aggregate form.....	111
4.14	Particle size distributions for PT110™, before and after 20 AB cycles.....	112

4.15	TEM image of HCV™ grade BN coated with alumina. This image is of a primary particle within a cross-section of an aggregate; there may be a slight angle on the particle, giving the appearance that the coating is thicker on the bottom than on the top.....	115
4.16	Viscosity versus RPM data. HCV™ grade BN particles; circles are uncoated data, squares are for particles coated with 20 AB cycles of alumina.....	119
4.17	Viscosity versus RPM data. Grade PT120™ BN particles; circles are uncoated data, squares are for particles coated with 20 AB cycles of alumina.....	120
5.1	Reactor system schematic.....	131
5.2	Sample dose scheme for providing reagents to fluidizing iron powders. The first dose is TMA, the second is H ₂ O.....	133
5.3	Fluidizing Fe particles. Image taken with laser imaging system. Average agglomerate size is $9.6 \cdot 10^{-5}$ m (96 μm).....	134
5.4	Particle magnetization versus applied field for $5 \cdot 10^{-6}$ m (5 μm) iron particles. The magnetization always goes through zero, regardless of increasing or	

decreasing field; this indicates that the particles are multi-domain and will have no net pole strength in the absence of an applied magnetic field.....137

- 5.5** TEM image of bare iron particle, no alumina coating. The dark region on the right is the particle, and the lighter crystalline region to its left is the native oxide.....138
- 5.6** Scanning TEM image of uncoated iron particle, showing the existence native oxide. The lighter region at the edge of the particle is oxygen-rich, indicative of a native iron oxide- probably α -Fe₂O₃.....139
- 5.7** Graph of u_{mf} versus pressure for fine iron powder with different surface conditions. Also shown is the operating point during fluidized bed coating experiments.....142
- 5.8** TEM image of $5 \cdot 10^{-6}$ m (5 μ m) iron particle coated with amorphous alumina.....148
- 5.9** HRTEM image of coated iron particle from the same coating batch as Figure 5.8, showing both alumina coating and native oxide.....149
- 5.10** Particle size distribution for fine iron particles. As the coating thickness increases, there is no significant change in the size distribution,

	indicating that the coating is not necking or binding the particles together.....	151
5.11	Mass gain at elevated temperature in an oxidizing environment for iron particles coated with several different numbers of AB cycles. The temperature ramp profile is also shown. Numbers indicate the number of AB cycles for a particular experiment.....	153
5.12	Mass gain at elevated temperature in an oxidizing environment for uncoated iron particles. The temperature ramp profile is also shown. The three experiments show an error of about 0.02 relative mass units.....	154
5.13	Mass gain at elevated temperature in an oxidizing environment for iron particles coated with 100 AB cycles. The temperature ramp profile is also shown. The four experiments show an error of about 0.07 relative mass units for 100 AB cycles.....	155
5.14	Magnetic moment at high applied field versus number of AB cycles for alumina- coated iron particles.....	157
A1.1	ALD dosing and fluidizing gas piping scheme. The valves from the MFC and each reagent are pneumatically controlled; the conductance limiters for the dosing lines are immediately after.....	171

A1.2	Diagram and photo of stainless steel reactor inside furnace.....	172
A1.3	Clamping mechanism. Bolts are as indicated. There is a third hold down bolt that cannot be seen in this picture.....	173
A1.4	Glass reactor top portion.....	174
A1.5	Bottom of top half of glass reactor, showing porous metal distributor plate installed with three screws.....	175
A1.6	Flowrate versus differential pressure for 4 conditions: no doses with a) main conductance limiter open, b) main conductance limiter shut, c) TMA dose, d) water dose.....	182
A1.7	Piping diagram for fine powders. O,1,3,4 and 5 are automatic isolation valves controlled by Labview; the numbering scheme was determined by the channels that each valve corresponds to on the NI computer card.....	184
A2.1	Front panel for “MFC Operations.vi”.....	191
A2.2	Back panel display of “MFC Operations.vi.”.....	192

A2.3	Front panel for “initial valve operator.vi.”.....	193
A2.4	Back panel of “initial valve operator.vi.”.....	194
A2.5	Front panel for “vacuumsavedatagood.vi.”.....	195
A2.6	Back panel for “vacuumsavedatagood.vi.”.....	196
A2.7	Front panel for “automatic valve operator.vi.”.....	197
A2.8	First part of the “automatic valve operator.vi” back panel, establishing initial conditions.....	198
A2.9	TMA dosing valve operations within “automatic valve operator.vi.”	199
A2.10	TMA dosing timing operations in “automatic valve operator.vi.”.....	200
A2.11	N ₂ purging of reactor after a TMA dose. Note the MFC setting in the orange box.	201
A2.12	Timing operation for N ₂ purging following a TMA dose.....	202

A2.13 Operations to secure N₂ flow and pump down the dosing header and reactor separately.203

A2.14 Timing operation for additional purge.....204

A2.15 Final panel for “automatic valve operator.vi.” This panel establishes the final conditions that the system is to be left in following an experiment.....205

PREVIEW

Chapter 1. Introduction

There is a current need to provide simple methods to place conformal, pinhole-free, nanoscale-thickness films on fine particles. Such processing can be done using atomic layer deposition (ALD) in a fluidized bed reactor, as will be shown in this thesis. This work is the first application of ALD to coat bulk quantities of fine powders. A fundamental understanding of the fluidization of fine cohesive particles at reduced pressure along with the ALD processing of these particles is the major focus of this thesis. The applications for such nanocoated particles are broad and can be found in many different areas of materials science including microelectronics, defense, biomedical, consumer products, advanced materials, and others.

Fluidized Bed Reactors

The use of fluidized beds to coat particles began in the 1960's to coat nuclear fuels [1]. In a fluidized bed, intimate contacting between a gas and all particles in the bed is obtained due to constant mixing of the particles by the gas. This leads to excellent heat and mass transfer characteristics within the bed of particles. Additionally, fluidized beds are typically scaleable with some simple and effective scaling equations [2].

There are many different sizes and shapes of powder particles. The fluidization characteristics of different types of powders have been defined, in loose terms, according to their size and density with the definition of Geldart A, B, C or D types [3]. Group C powders are difficult to fluidize due to their cohesive nature.

Fine powders, those considered Geldart C powders, self-aggregate into larger particles when exposed to gas flows in a fluidized bed apparatus, even under vacuum conditions [4-6]. These light aggregates are formed by Van Der Waals forces [7], and the size of the aggregates may depend on several factors such as individual particle type, size, shape, and density, gas flowrate, and vibration applied to the bed.

In the late 1970's, some work was done in the field by researchers studying fluidization at pressures that were sub-atmospheric. The first such papers described a classical model used to calculate the minimum fluidization velocity for pressures less than ~ 4000 Pa (30 Torr) but greater than ~ 500 Pa (4 Torr) [8]. In this paper, the authors were using large glass beads as their powder. Geldart and colleagues then described fluidization of Group A powders under a vacuum [9], albeit only down to $2 \cdot 10^4$ Pa (150 Torr).

Low pressure fluidization does not follow normal flow patterns. This is due to the fact that as the pressure is reduced, the fluidizing gas is no longer in a laminar flow regime. Rather, the gas is in a condition known as "slip flow" where the viscous forces acting upwards on the particles are reduced due to an increase in the gas molecular mean free path [10]. Because of this, the usual equations to calculate the minimum fluidization velocity, u_{mf} , may no longer be valid [2].

Experimental results show that the process of fluidizing fine particles usually involves plugging, channeling, disrupting, and agglomerating [4, 5]. When fluidized, the entities fluidized generally consist of particle aggregates varying in size from the largest at the bottom of the bed (some even defluidized) to the smallest at the top (some even unassociated to discrete particles). Easiest to fluidize are the aggregates